

Simulation studies of the information content of muon arrival time observations of high energy extensive air showers

I. M. Brancus¹, H. Rebel², M. Duma¹, A. F. Badea¹, C. Aiftimiei¹, and J. Oehlschlaeger²

¹IFIN-HH Bucharest, P.O.B.MG-6, 76900 Bucharest, Romania

²Forschungszentrum Karlsruhe, Institut f. Kernphysik, Postfach 3640, 76021 Karlsruhe, Germany

Abstract. On basis of detailed Monte Carlo simulations of high energy Extensive Air Showers, using the EAS simulation code CORSIKA, the information potential of muon arrival time studies has been explored. Muon arrival time distributions and EAS time profiles have been analysed up to 320 m distances from the EAS centre for proton, oxygen and iron induced showers. Special attention is focussed to the model dependence and mass discriminating features, scrutinized for three energies ranges, (1.-1.78) 10^{15} eV, (1.-1.78) 10^{16} eV and (1.78-3.16) 10^{16} eV. Non-parametric statistical inference methods have been applied in the analysis of multi-dimensional distributions and of the correlations of the EAS time parameters with different other EAS observables. Local muon arrival times referring to the first registered muon indicate a good mass separation when correlated with the local muon density and the shower age, especially at larger distances from the shower core. Global muon arrival times, which refer to the arrival of the shower core and represent also the curvature of the EAS disk, exhibit a slightly improved mass separation quality.

core ("global" arrival times):

$$\Delta\tau_{\mu}^n = \tau_{\mu}^n(R_{\mu}) - \tau_c \quad (1)$$

When the arrival time τ_c is difficult to determine with sufficient precision, "local" times are considered, which refer to the foremost muon, locally registered by the detector:

$$\Delta\tau^n(R_{\mu}) = \tau_{\mu}^n(R_{\mu}) - \tau_{\mu}^1(R_{\mu}) \quad (2)$$

The single relative arrival time distributions can be characterised by the mean values $\Delta\tau_{mean}$, and by quantiles $\Delta\tau_q$ like the median $\Delta\tau_{0.50}$, the first quartile $\Delta\tau_{0.25}$ and the third quartile $\Delta\tau_{0.75}$ (Antoni et al., 2001). Their mean values and dispersion (standard deviations) represent the time profile of the EAS muon component. Recently the temporal EAS structure has been studied in dependence on the shower size N_e , the muon number N_{μ} , or the truncated muon number N_{μ}^{tr} in KASCADE experiment (Antoni et al., 2001). The present analysis, based on simulations neglecting the detector response, explores the basic information which is provided by the time observables and their correlations with other EAS observables, in view of the discrimination of the primaries mass and of the hadronic interaction model.

1 Introduction

The temporal structure of the muon component of Extended Air Showers (EAS) is of great interest for a detailed understanding of the EAS structure, since it reflects the longitudinal EAS development (Linsley et al., 1961; Rebel et al., 1995). Muon arrival distributions, observed in particular at large distances from the shower axis map the distributions of the production heights via the time-of-flight of the muons from the decay loci of the charged pions which are produced by hadronic collisions along the shower axis. Arrival times $\tau_{\mu}^1, \tau_{\mu}^2, \tau_{\mu}^3, \dots$ of muons, registered by timing detectors at a distance R_{μ} from the shower centre have to refer to a well defined zero-time, usually the arrival time τ_c of the shower

2 Time profiles of the EAS muon component

For calculating the time profiles the EAS development has been simulated by the Monte Carlo program CORSIKA (Heck et al., 1998), invoking different models for the hadronic interaction, QGSJET, VENUS, and SIBYLL, and using the NKG approximation for the electron-photon component and the full Monte Carlo EGS simulations (Antoni et al., 2001). 500 proton and 500 iron induced EAS of the primary energy of 10^{15} eV and of vertical incidence have been analysed for a radial range up to 150 m, and the muon arrival time distributions and time profiles (bins with $\Delta R_{\mu} = 10$ m) of the muon component ($E_{\mu} \geq 2.4$ GeV) have been constructed.

Fig.1 displays the time profiles for the median distributions and for median divided by the average density $\rho_{\mu}(R_{\mu})$

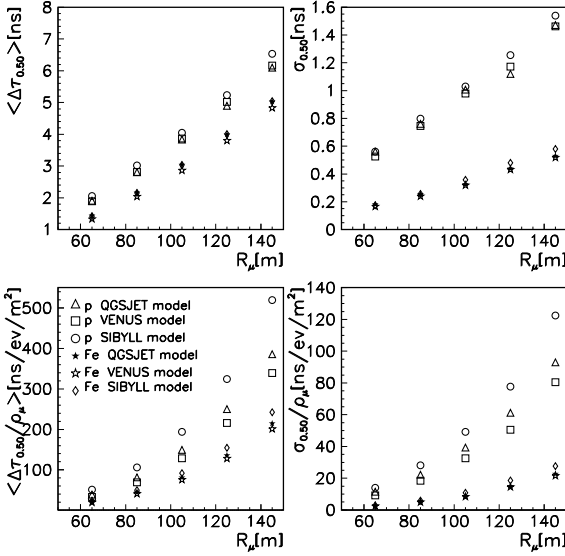


Fig. 1. Simulated muon profiles for the time distributions and the standard deviations by $\Delta\tau_{0.50}$ and $\Delta\tau_{0.50}/\rho_\mu$, for two primaries p and Fe and for three models, QGSJET, VENUS, and SIBYLL.

of muons in the corresponding R_μ -bin, for the two different primaries p and Fe of the energy 10^{15} eV and comparing three different hadronic interaction models. The use of the observables $\Delta\tau_q(R_\mu)/\rho_\mu(R_\mu)$ results in some improvement of the mass discrimination, but especially for the discrimination of different models, the lateral distribution of the muons is contributing to the discriminative power.

For higher energies, $(1.78-3.16) \cdot 10^{16}$ eV, and for each class of primaries, p, O, and Fe, 50 showers have been generated for QGSJET model on extended radial ranges up to 310 m.

Fig.2 displays the profiles of $\Delta\tau_q/\rho_\mu$, resulting in a similar behaviour for both local and global times with a better separation of primaries with increasing distance from the shower core.

3 Non-parametric statistical analysis

The non-parametric statistical methods enable the study of multidimensional observables-distributions to associate the single observed events to different classes (in our case to proton, oxygen or iron primaries) by comparing the observed events with the model distributions without using a pre-chosen parameterisation (Chilingarian, 1989). For each class of primaries, p, O and Fe, 200 showers with energies in the range $(1.-1.78) \cdot 10^{15}$ eV, 100 showers with energies in the range $(1.-1.78) \cdot 10^{16}$ eV and 50 showers with energies in the range $(1.78-3.16) \cdot 10^{16}$ eV have been generated for QGSJET and VENUS models, and the multidimensional distributions of various EAS observables have been analysed using the Bayesian approach.

Fig.3 displays the probability distribution for $\Delta\tau_{0.50}(R_\mu)/\rho_\mu(R_\mu)$ for median local times, at 3 different

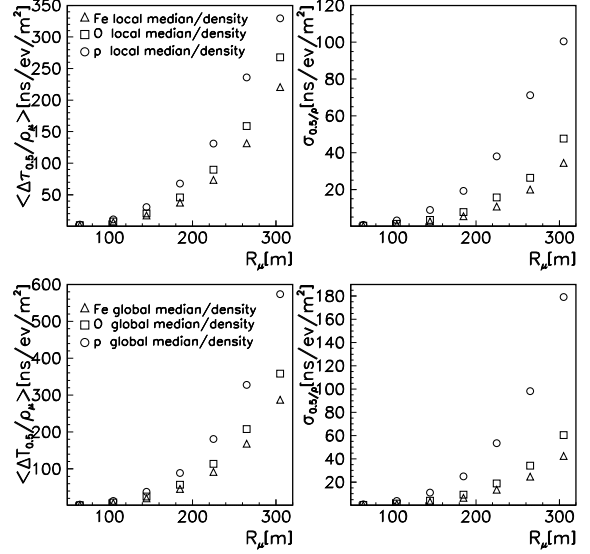


Fig. 2. Simulated muon profiles for the $\Delta\tau_q/\rho_\mu$ distributions and the standard deviations of the local and global median values, for the three primaries p, O, Fe.

radial distances, whose overlaps indicate the expected improved separation by the combination time/density.

The values of the classification and misclassification probabilities of an EAS event to be associated to a particular class are presented in Figs. 4, 5 and listed in the tables.

The notation is: $\Delta\tau_{0.50}(R_x)$ is the median arrival time in the range R_x , $x=A,B,C$, where $90 \text{ m} \leq R_A < 100 \text{ m}$, $180 \text{ m} \leq R_B < 190 \text{ m}$, and $260 \text{ m} \leq R_C < 270 \text{ m}$; $\rho_\mu(R_x)$ is the density in the radial range R_x .

Fig.4 shows the classification and misclassification probabilities for various combinations of EAS observables for QGSJET model at incident energy $(1.78 - 3.16) \cdot 10^{16}$ eV. The quantity muon arrival time/muon density gives a better discrimination than each separated quantities, similar by taking the correlations of two observables, muon arrival time and muon density. The use of muon *global* times instead of *local* times brings a slightly improved classification. For better mass discrimination we have to look for correlations of muon arrival times with N_e , N_μ^{tr} , and the shower age.

Fig.5 displays the comparison of the classification and misclassification probabilities using the correlation of the observation of the third quantile with other shower observables; the best result is given by correlating $\Delta\tau_{0.75}$ with the age and N_μ^{tr} .

Tab. 1 presents the classification and misclassification probabilities for various combinations of EAS observables at high energies, 50 showers for each class: p, O, Fe, $(1.78-3.16) \cdot 10^{16}$ eV.

The comparison of the muon arrival times at different radial distances indicates an improved mass discrimination for larger distances.

Tab. 2 gives the classification and misclassification prob-

Mode	P ↓			O ↓			Fe ↓		
	P	O	Fe	P	O	Fe	P	O	Fe
N_e	.56	.34	.10	.19	.44	.37	.00	.17	.83
$N_e - \Delta\tau_{0.50}^A/\rho_\mu^A$.73	.23	.04	.09	.63	.28	.00	.19	.81
$N_e - \Delta\tau_{0.50}^A/\rho_\mu^A - \Delta\tau_{0.50}^C/\rho_\mu^C$.72	.24	.04	.10	.64	.26	.00	.15	.85
$N_e - \Delta\tau_{0.50}^A/\rho_\mu^A - \Delta\tau_{0.50}^B/\rho_\mu^B - \Delta\tau_{0.50}^C/\rho_\mu^C$.77	.20	.03	.08	.66	.26	.00	.15	.85
N_μ^{tr}	.43	.31	.26	.10	.35	.55	.00	.28	.72
$N_\mu^{tr} - \Delta\tau_{0.50}^A/\rho_\mu^A$.69	.28	.03	.05	.63	.32	.00	.13	.87
$N_\mu^{tr} - \Delta\tau_{0.50}^A/\rho_\mu^A - \Delta\tau_{0.50}^C/\rho_\mu^C$.70	.26	.04	.06	.65	.29	.00	.13	.87
$N_\mu^{tr} - \Delta\tau_{0.50}^A/\rho_\mu^A - \Delta\tau_{0.50}^B/\rho_\mu^B - \Delta\tau_{0.50}^C/\rho_\mu^C$.73	.23	.04	.05	.68	.27	.00	.17	.83

Table 1. The classification and misclassification probabilities inferred from different combinations of shower observables: N_e and N_μ^{tr} and correlating with $\Delta\tau_{0.50}/\rho_\mu$ at different radial distances for the modes: only one observable, N_e , respectively N_μ^{tr} ; two observables by adding $\Delta\tau_{0.50}(R_A)/\rho_\mu(R_A)$; three observables by adding $\Delta\tau_{0.50}(R_C)/\rho_\mu(R_C)$; four observables by adding $\Delta\tau_{0.50}(R_B)/\rho_\mu(R_B)$.

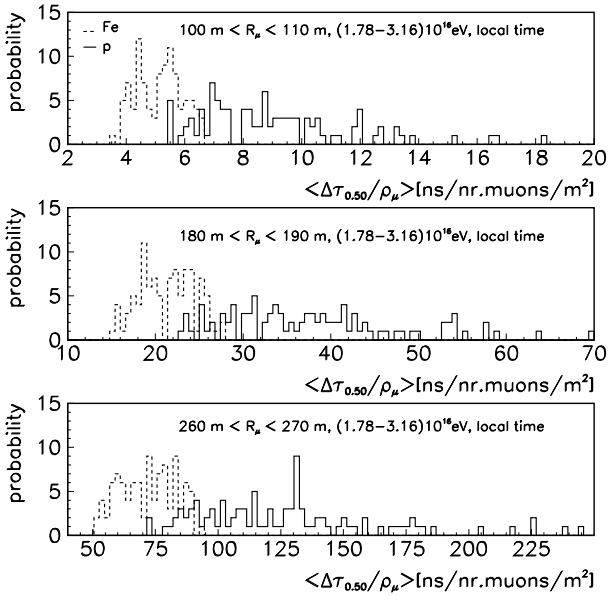


Fig. 3. The probability density distributions for $\Delta\tau_q/\rho_\mu$ corresponding to proton and iron EAS primaries, for three different radial distances from the shower core.

abilities at different incident energies, by correlating the shower age $\Delta\tau_{0.50}(R_A)/\rho_\mu(R_A)$ displaying an improved discrimination for higher energies.

Energy	P ↓			O ↓			Fe ↓		
	P	O	Fe	P	O	Fe	P	O	Fe
$1 \cdot 10^{15}$.70	.28	.01	.14	.56	.30	.00	.19	.81
$1 \cdot 10^{16}$.73	.25	.02	.09	.71	.20	.00	.21	.79
$1.78 \cdot 10^{16}$.73	.24	.03	.06	.72	.22	.00	.07	.93

Table 2. The classification and misclassification probabilities by correlating age, $\Delta\tau_{0.50}(R_A)/\rho_\mu(R_A)$ for different energy ranges, $(1-1.78) \cdot 10^{15}$ eV, $(1-1.78) \cdot 10^{16}$ eV, and $(1.78-3.16) \cdot 10^{16}$ eV.

Tab. 3 compares the classification and misclassification probabilities using QGSJET and VENUS model, by correlating the age, $N_e - \Delta\tau_{0.50}(R_A)/\rho_\mu(R_A)$.

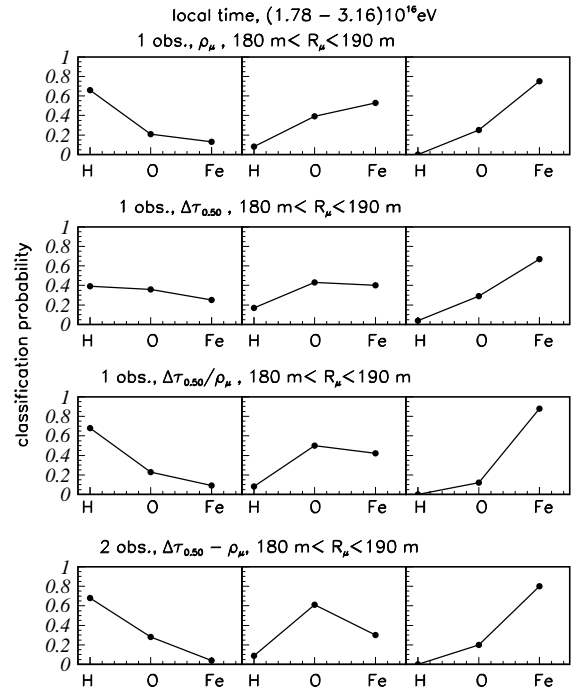


Fig. 4. The classification and misclassification probabilities for different observation modes.

Model	P ↓			O ↓			Fe ↓		
	P	O	Fe	P	O	Fe	P	O	Fe
QGS	.75	.23	.01	.08	.68	.23	.00	.15	.84
VEN	.80	.18	.01	.08	.70	.22	.00	.12	.88

Table 3. The classification and misclassification probabilities by correlating age $N_e - \Delta\tau_{0.50}(R_A)/\rho_\mu(R_A)$ for the primary energy $(1-1.78) \cdot 10^{16}$ eV with the two different interaction models QGSJET and VENUS.

4 Conclusions

The present studies have been focussed to explore the information carried by EAS time observables and their correlations in view of features discriminating the mass of the cos-

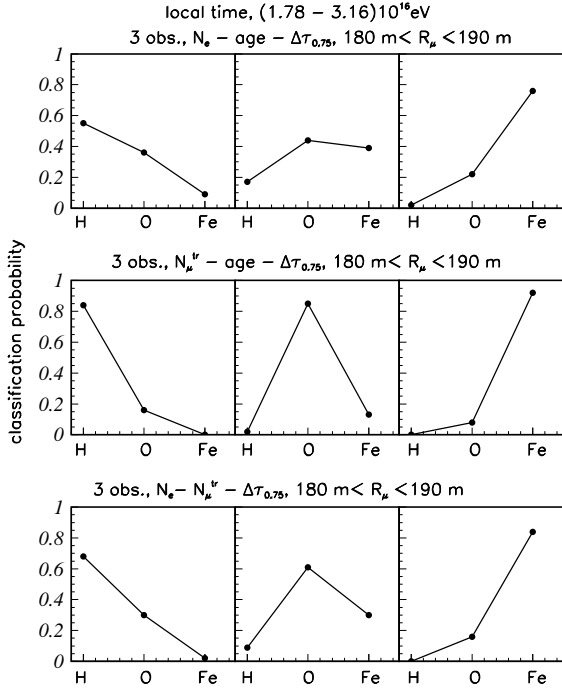


Fig. 5. The classification and misclassification probabilities correlating the observation of muon arrival times with N_e , N_μ^{tr} and the shower age.

mic primary and different hadronic interaction models. Advanced non-parametrical statistical methods based on Bayesian decision rules have been applied to scrutinise the EAS observables and to specify quantitatively the results:

1. The correlations of the local muon arrival time variables with the local muon density improves the true classification rate and discrimination features. It turns out that the correlation can be replaced by a single parameter: $\Delta\tau_q/\rho_\mu$. The classification gets improved by the cor-

relation with the shower age, the shower size N_e , and N_μ^{tr} .

2. Correlating the observation of $\Delta\tau_q/\rho_\mu$ for different radial distances, the mass discrimination of the primaries is only slightly improved, different from our previous result (Brancus et al., 1997) analysing the (global) arrival times of the foremost muon.
3. Comparing the classification rates for different muon arrival time quantities, the VENUS model leads to better results than the QGSJET one.

From the present results an enhancement of the discriminative features may be expected at larger distances from the shower core ($> 150 \text{ m}$) and to higher primary energies ($> 10^{16} \text{ eV}$). The finding is of actual interest in view of the current efforts of the KASCADE collaboration to extend the detector array to a larger area: KASCADE GRANDE.

Acknowledgements. One author (I.B.) acknowledges the support by a grant from the Deutsche Forschungsgemeinschaft and the Forschungszentrum Karlsruhe for the hospitality, providing the possibility to perform detailed analyses of the information carried by muon arrival times observations.

References

- Antoni, T., et al., KASCADE Collaboration, *Astropart. Phys.* 14, 245, 2001.
- Antoni, T., et al., KASCADE Collaboration, *Astropart. Phys.* 15, 149, 2001.
- Brancus, I.M., et al., *Astropart. Phys.* 7, 343, 1997.
- Chilingarian, A.A., *Comp. Phys. Comm.* 54, 381, 1989; Chilingarian, A.A., ANI Reference Manual, 1999.
- Heck, D., et al., Report FZKA 6019, Forschungszentrum Karlsruhe, 1998.
- Linsley, J., et al., *Phys. Rev.* 92, 485, 1961.
- Rebel, H., et al., *Journ. Phys. G: Nucl. Part. Phys.* 21, 451, 1995.